ORIGINAL ARTICLE

Cold formability of friction stir processed 5754-H111 and 6082-T6 aluminum alloys: an experimental and numerical study

Alessia Teresa Silvestri[1] · Gianluca Parodo[2] · Francesco Napolitano[1] · Andrea El Hassanin[1] · Fabio Scherillo[1] · Luca Sorrentino[2] · Antonino Squillace[1]

Abstract

Aluminum has become increasingly important in the automotive sector due to its ability to reduce vehicle weight without compromising structural performance. However, joining different types of aluminum alloys can be challenging due to their different thermal and mechanical characteristics. Concurrently, friction stir processing (FSP) is a material processing technique that has garnered considerable attention for its versatility and industrial applicability, and it may represent a preliminary phase to correctly perform friction stir welding, which is a welding technology used to join different types of aluminum alloys. In this context, this study presents an extensive experimental campaign of FSP performed on 5754-H111 and 6082-T6 alloys, varying two rolling directions and four welding speeds. The processed materials were characterized, including cupping and tensile tests, microstructure analysis, and a correlation between welding parameters, microstructure, and mechanical resistance. In addition, a numerical method was proposed to simulate the Erichsen tests and predict the formability of the materials, before and after the FSP processes. The results showed that both alloys exhibited good formability after the FSP process, but with different behavior. AA6082 underwent internal decohesion and dynamic recrystallization, resulting in the absence of defects and an increase in ductility and cold formability. AA5754 experiences more difficulty with material flow during FSP and showed the presence of tunnel defects in all analyzed process conditions. However, the alloy 5754 did not undergo softening and had comparable mechanical behavior and cold formability to the base material. These results were validated by the numerical method proposed.

1 Introduction

In the last few years, aluminum has been one of the favorite choices to produce a large variety of components in the automotive sector. Most notably, aluminum is a suitable alternative to replace other metals to reduce the weight of the vehicles while avoiding loss of structural performance. Therefore, the aluminum percentage, in terms of volume and weight, is increasing in the whole vehicle and involves a great variety of alloys with the aim of taking full advantage of their peculiar thermal and mechanical characteristics [1].

Furthermore, the growth of hybrid and full electric vehicle production pushes for a further increase in aluminum use since it is present in the battery case components to enhance thermal exchange and cooling [2, 3]. This has led to the study of new setup configurations and the investigation of the best joining techniques, as this has an influence on the whole vehicle manufacturing in various manners [4]. Aluminum components employed in the automotive sector are mainly in the form of casting workpieces, extruded items, or rolling sheets. In previous research, the friction stir welding (FSW) joining of two heterogeneous components was studied, both casting and extruded [5], which is a common occurrence in the modern battery pack. Aluminum alloys welded using the FSW process have reached significant importance in the battery pack assembly, due to their ability to prevent electromagnetic interferences. The utilization of

✉ Alessia Teresa Silvestri
alessiateresa.silvestri@unina.it

1 Department of Chemical, Materials and Industrial Production Engineering, University of Naples "Federico II", P.le Tecchio 80, 80125 Naples, Italy

2 Department of Civil and Mechanical Engineering, University of Cassino and Southern Lazio, 03043 Cassino, Italy

these alloys in conjunction with this specific welding process allows to create the whole electrical setup, followed by the sealing of the metallic case. Other conventional or innovative technologies, such as those using laser or electrical beams, might encounter some issues that could damage the electrical parts, considering the involved temperature or the electromagnetic flow of the process [6, 7]. This type of joining is very challenging because the two alloys have very different thermal characteristics and accurate assembly is needed. Another arduous and recurrent occurrence regards the joining of cold rolled sheets (AA5xxx) and hot rolled sheets (AA6xxx). These alloys, in fact, have different heat absorption and different responses to the microstructure modifications [8], in particular when the design requirements impose to form the sheets after the welding process [9, 10].

The formability of the raw aluminum alloys, 5xxx and 6xxx, is deeply studied in literature [11]. More recently, other authors began to investigate the issues related to the formability after the process. Some researchers investigated the formability of the welded workpieces after the application of heat treatment, in the case of hydraulic tubes under pressure [12], and on 2024-O aluminum alloy rolled plates [13, 14]. Patel et al. designed an experimental campaign with two aluminum alloys having dissimilar mechanical characteristics with the aim of investigating the influence of each process parameter on the tailor welded blank (TWB) formability [15]. Different authors studied the formability of the TWB AA6xxx and AA5xxx, having 1 mm thickness, after FSW [16, 17]; instead, Tayebi et al. used the single point incremental forming to verify the formability of the AA6xxx and AA5xxx FSWed sheets [18]. In many research works, the Erichsen cupping test was used in the perspective to perform the formability assessment. Akterer et al. measured the formability of the FSW joint between aluminum alloys and incremental formed steel [19]. Pang et al. investigated the response of AA7075 foam precursor, prepared by friction stir processing, and then subjected to cupping tests [20].

In this scenario, the objective of this research study is to provide a comprehensive characterization of the formability and mechanical resistance of aluminum rolled sheets after friction stir processing (FSP). In addition, a simplified numerical approach is proposed to simulate the Erichsen tests and predict the formability of the materials, before and after the FSP processes. The sheets are made by two different aluminum alloys, AA5754-H111 and AA6082-T6, with 2 mm thickness, the choice of these alloys is based on their versatility, which made them highly used in the automotive sector. As a matter of fact, some researchers report studies on the effects of FSW in 5754-H111 joining for automotive production [21–23]. Yürük et al. proposed a mechanical and microstructural assessment after FSW of 5754-H111

aluminum alloy with the aim to perform welding in the automotive and shipbuilding industry [24]. Rodríguez-Millán et al. studied the effect of the perforation under normal impact by conical, hemispherical, and blunt projectiles on 5754-H111 and 6082-T6 aluminum alloys due to their large use in the automotive and naval sector [25]. The investigation also includes studying the influence of process parameters, i.e., the welding directions, the heat inputs generated during the process, and the surfaces subjected to force during the Erichsen cupping tests. This is accomplished by considering welding directions parallel and perpendicular to the rolling direction and by varying the travel speed in order to achieve lower and higher heat inputs. Specifically, these variations result in two defined conditions termed "hot" and "cold." Each condition was tested at both the extrados and intrados in the Erichsen tests. The results of cupping and tensile tests and the microstructure and fracture analyses are reported in order to evaluate the effect of the FSP on the single material, give the basis for a future implementation of FSW, and solve the issues that traditionally affect the welded joint, such as porosity and blowhole generated by the melting and solidification which happen in the welding zone [26]. Furthermore, a correlation between welding parameters, specific microstructure, and mechanical resistance is presented.

2 Materials and methods

2.1 Materials and experimental campaign

The materials used are 2-mm-thick sheets of Al–Mg alloy AA5754-H111 and AL–Mg-Si alloy AA6082-T6. The samples are rolled plates of $200 \times 100 \times 2$ mm^3 dimension. FSP was carried out in the center of the rectangular plates according to the perpendicular and parallel directions with respect to the rolling direction. The FSP tool is a trifluted one; it has a shoulder diameter of 8 mm, a pin diameter of 2.7 mm, and a pin length of 1.8 mm (provided by FPT industries). The experiments were conducted on a vertical milling machine using a customized fixture and the tool mentioned above. The process parameters in this study are listed in Table 1. The process parameters were chosen based on the studies of Kim et al. and Yi et al. [27, 28]. Indeed, as explained in an authors' previous work [5], a travel speed range value is obtained by considering the tool's geometry and the material's thermal characteristics and fixing the rotation speed. In particular, 38–118 mm/min is the range found for the travel speed for AA6082 sheets and 33–101 mm/min for the AA5754. By choosing the minimum and the maximum values of these ranges for each material considered, the related heat input can be considered, respectively, maximum and minimum. For these reasons, the correlated processing

conditions will be indicated as "hot" (minimum travel speed value) and "cold" (maximum travel speed value).

The processing direction has been considered aligned and perpendicular to the rolling one to investigate its effects on the microstructural and mechanical properties. Both directions are indicated in Fig. 1, where the rolling directions are indicated as "rolling direction 1" if it is aligned with the welding direction and "rolling direction 2" if it is perpendicular to the welding direction. In summary, four different processing conditions for the two materials have been considered for a total of 8 FSP experiments.

2.2 Characterization procedures

Samples for metallographic and microhardness analysis were obtained by cutting the welded plates to investigate the cross-section in the direction perpendicular to the FSP one. Then, the samples were mounted and polished according to the metallographic procedure [29–31]. To measure the hardness of the specimens, Vickers microindentation tests were performed using a test load of 100 gf and a dwell time of 15 s. Three lines of indentation were made, hereinafter indicated as bottom, core and top, as shown in Fig. 2, considering a distance equal to 0.75 mm in the vertical direction and a distance equal to 1 mm in the horizontal direction. However, more indentations were made horizontally, reducing the space between two adjacent indentations, in the 6082-T6 samples, considering the more variable values of microhardness and so to report a more precise trend, as discussed in the further section. For metallographic analysis, the specimens were electrochemically etched using a solution made of 5 ml of HBF_4 (48 wt%) in

Table 1 Experimental conditions and main FSP parameters

No conditions and ID samples	Materials	Rotation speed (rpm)	Travel speed (mm/min)	Tilt angle (°)	Processing direction	Processing conditions
1: 6-Perp-Hot	6082-T6	1350	38	2	Perpendicular	Hot
2: 6-Par-Hot	6082-T6	1350	38	2	Parallel	Hot
3: 6-Perp-Cold	6082-T6	1350	118	2	Perpendicular	Cold
4: 6-Par-Cold	6082-T6	1350	118	2	Parallel	Cold
5: 5-Perp-Hot	5754-H111	1350	33	2	Perpendicular	Hot
6: 5-Par-Hot	5754-H111	1350	33	2	Parallel	Hot
7: 5-Perp-Cold	5754-H111	1350	101	2	Perpendicular	Cold
8: 5-Par-Cold	5754-H111	1350	101	2	Parallel	Cold

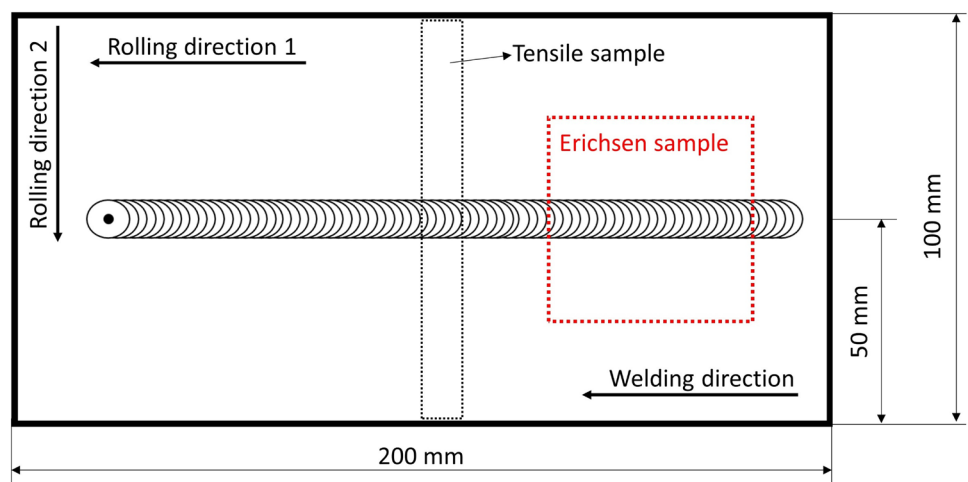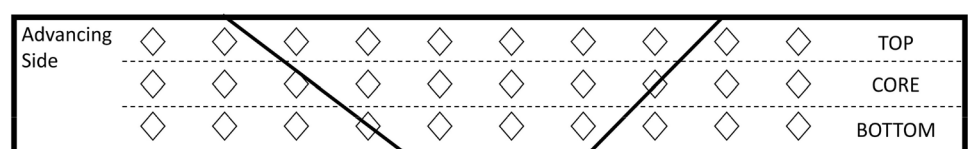**Fig. 1** Schematic representation of processing directions and orientation of samples

Fig. 2 Schematic representation of zone investigated during the microhardness tests

200 ml of H$_2$O and applying 20 V for 1 min; the observations were made by means of a polarized light microscope. The mechanical properties of the joints were also evaluated by tensile tests. Specimens for tensile tests were prepared perpendicular to the welding direction as schematically shown in Fig. 1 (black dotted rectangle indicated as "tensile sample"). Uniaxial tensile tests were carried out by using a Galdabini QUASAR 50 testing machine, which is equipped with a 50-kN load cell; tests were performed at room temperature according to standard ASTM E8 [32] and with a testing speed set to 3 mm/min, and the results were compared to the base materials ones. Three specimens for each FSP configuration were tested.

To measure the ability of the sample to undergo plastic deformation in stretch forming, Erichsen cupping tests were carried out according to the ISO 20482 [33], which is valid for sheets having a thickness up to 2 mm and a width of 90 mm or greater. The procedure involves forming an indentation by pressing a punch with a spherical end against a specimen clamped between a die and blank holder until a through crack appears. A through crack is defined as a crack that runs through the entire thickness of the specimen and is wide enough to allow the passage of light through a part of its length. Samples with $55 \times 55 \times 2$ mm^3 have been obtained from the FSP sheets, as schematically shown in Fig. 1 (red dotted square indicated as "Erichsen sample"). Three specimens have been tested for each of the configuration described above, and putting the welding line both at the intrados and at the extrados, for a total of 48 Erichsen tests (4 processing conditions, 2 materials, 3 replicas and 2 Erichsen test configurations). The blank holder force is about 10 kN, and the results are reported as cup height, intended as the measured depth of the indentation.

2.3 Numerical analysis

In this work, a simplified approach is proposed to simulate the effect of FSP on metal sheet formability. Specifically, the numerical simulations of Erichsen tests were carried out using the commercial software PAM-STAMP, developed by Esi Group. The geometry of the tools was set in accordance with ISO 20482, while an axisymmetric configuration was adopted in order to reduce the number of elements. The meshes consisted of three- and four-node Belytschko-Tsay shell elements.

For better clarity, the mesh for the tools and the sample used is shown respectively in Fig. 3a and b. Specifically, 5865 3-node elements and 10,217 4-node elements were used for die, 3060 3-node elements and 7004 4-node elements for blankholder, and 816 3-node elements and 9350 4-node elements for punch. In total, 160,082 elements, 10,064 elements, and 10,166 elements were used, respectively, for die, blankholder, and punch. The specimen mesh consisted of 31,812 3-and 4-node Belytschko-Tsay shell elements, and it was divided into 3 zones, as shown in Fig. 4. In fact, in order to simplify the numerical analysis, it has been made the hypothesis that the area subjected to FSP (represented by the central zone of the specimen) presented a variation of physical state due to a "reset" of the hardening effects and aging in the central zone. This hypothesis is plausible since the treatment involved a recrystallization and a solution of the precipitates. As a result, the samples were simulated as tailor welded sheets made of three different materials (Fig. 4). In the case of base sheet, the three materials were identical, while in the case of treated sheets, the three materials were different.

For simulations, Hill '48 quadratic yield criterion was used for considering anisotropy [34], which can be described with the following equation:

Fig. 3 Mesh adopted for Erichsen test simulations: **a** tools; **b** specimen
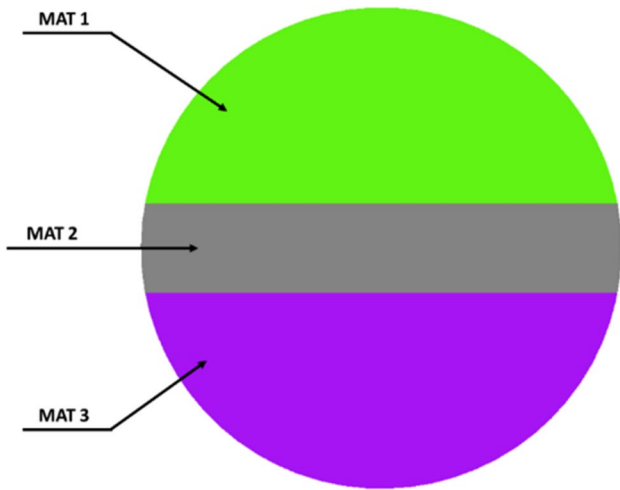
a)

b)
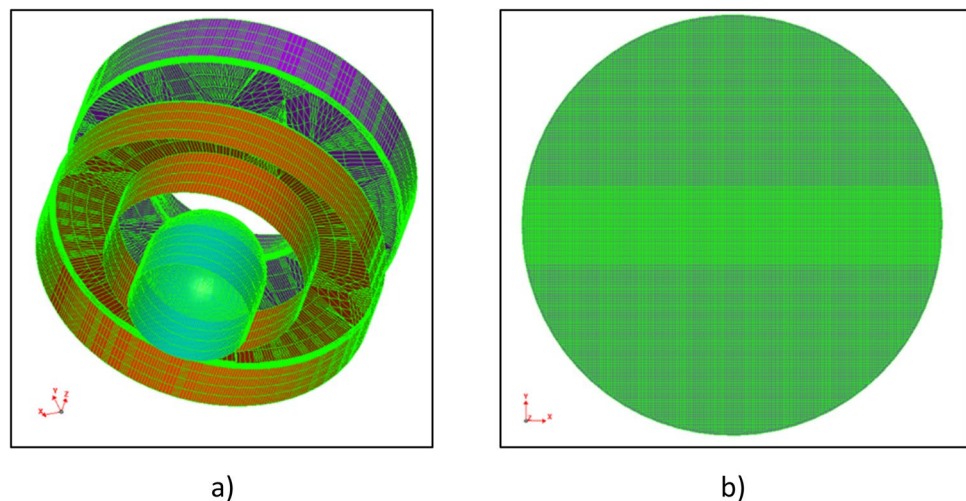
Fig. 4 Three zones used for modeling the Erichsen specimen subjected to FSP

Table 2 Anisotropic properties of AA5754-H111 adopted for simulations [35]

R_0	R_{45}	R_{90}
0.60	0.87	0.65

Table 3 Anisotropic properties of AA6082-T6 adopted for simulations [36]

F	G	H	N
0.378	0.662	0.338	1.205

$$F(\sigma_{yy} - \sigma_{zz})^2 + G(\sigma_{zz} - \sigma_{xx})^2 + H(\sigma_{xx} - \sigma_{yy})^2$$
$$+ 2L\sigma_{yz}^2 + 2M\sigma_{zx}^2 + 2N\sigma_{xy}^2 = 1$$

where x, y, and z are the orthogonal axes of orthotropy, and F, G, H, L, M, and N are material constants; σ_{xx} and σ_{yy} are the in-plane stresses, σ_{zz} is the out-of-plane stress, while σ_{yz}, σ_{zx}, and σ_{xy} are the shear stresses.

Since these were sheet metal forming processes, it was possible to assume plain stress conditions. In this way, the out-of-plane shear forces became zero ($\sigma_{yz} = \sigma_{zx} = 0$) and the out-of-plain principal stress became zero ($\sigma_{zz} = 0$). So, the yield criterion became as follows:

$$(F + H)\sigma_{yy}^2 + (G + H)\sigma_{xx}^2 - 2H\sigma_{xx}\sigma_{yy} + 2N\sigma_{xy}^2 = 1$$

If the F, G, H, and N coefficients were unknown, it is possible to calculate them starting from the Lankford coefficients in 0, 45, and 90 directions with respect to the rolling one:

$$F = \frac{R_0}{R_{90}(1 + R_0)}; G = \frac{1}{1 + R_0}; H = \frac{R_0}{1 + R_0}; N = \frac{(R_0 + R_{90})(1 + 2R_{45})}{2R_{90}(1 + R_0)}$$

Table 4 Parameter values for the two O-state alloys used for simulations

	K [MPa]	n [-]	ε_0 [-]	Ref
AA5754-O	477	0.307	0.0095	[37]
AA6082-O	290	0.096	-	[38]

The material parameters related to AA5754-H111 are reported in Table 2, while the material parameters related to AA6082-T6 are reported in Table 3.

Downstream of the FSP, it was assumed that due to recrystallization and solution, the anisotropy of the crystalline structure and the presence of fine precipitates were lost. As a result, it could be assumed that, downstream of the FSP, the central zone of the specimen changes to a physical state O and that the characteristics of that zone may be assimilated to an isotropic material. So, the hardening of AA6082-O has been modeled by the Swift hardening model:

$$\sigma = K(\varepsilon_0 + \varepsilon_p)^n$$

where K and n represented, respectively, the strength coefficient and hardening index, while ε_0 and ε_p represented the elastic strain and the plastic strain. For alloy AA5754-O, an exponential hardening law has been adopted:

$$\sigma = K\varepsilon_p^n$$

For completeness, the parameter values for the two O-state alloys used for simulations are given in Table 4.

Instead, forming limit curves were taken from literature both for AA5754 [37, 39] and AA6082 [36, 38, 40]. The effect of friction has been modeled using the Coulomb friction relation:

$$f_t = \mu f_n$$

where f_t and f_n represented, respectively, the tangential force and the normal force, while μ indicated the coefficient of friction. The value of the latter has been set at 0.12, in line with what is reported in the scientific literature [41].

The boundary conditions consisted of a clamping of the die in x, y, and z directions, of a force applied to the blankholder in the z-direction equal to 500 kN (needed only to avoid sliding of the specimen between the die and blankholder) and in a constant speed in z-direction imposed to the punch and equal to 2 mm/ms. This choice is only numerical: In fact, being a cold forming, the effects of the strain rate could be neglected.

3 Results and discussion

3.1 Experimental results

The macrographies of the friction stir–processed materials are reported in Figs. 5 and 6; the appearance is typical of the employed technology. It is possible to note the typical nugget in the central zone, where the combined effect of heat and deformation caused a complete recrystallization of the metal. On the side of the nuggets are the affected zones, and these zones differ considerably for the two alloys.

For example, looking at Fig. 5c, the 6082 alloy has an elongated microstructure in the rolling direction far from the welded zone, and this kind of microstructure remains unchanged up to the immediate proximity of the nugget,
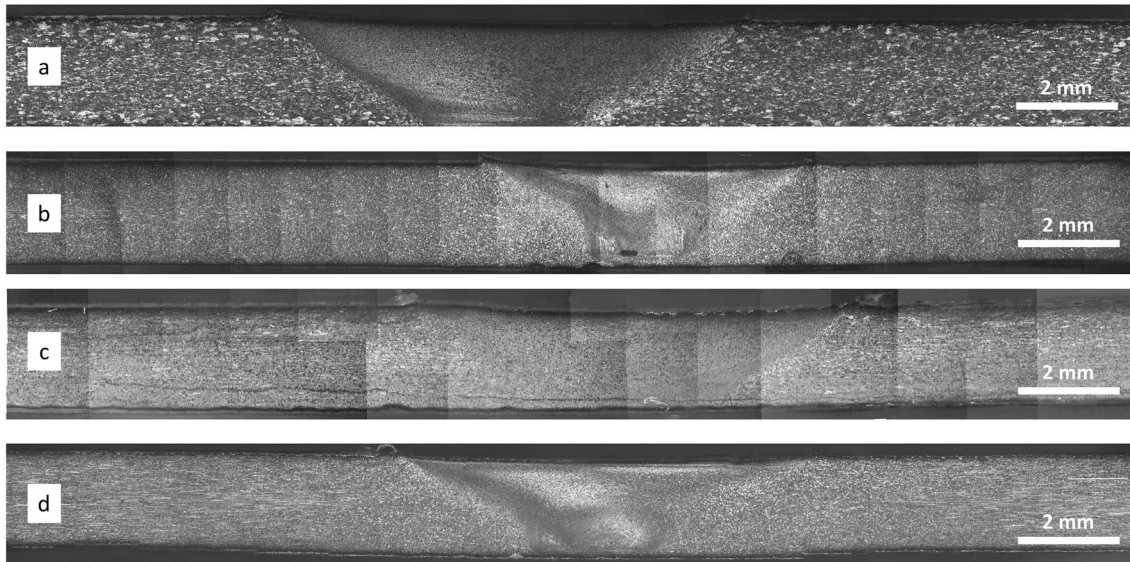
Fig. 5 Macrographies of FSP 6082 and 5754 alloys in hot conditions: **a** 6082 parallel, **b** 5754 parallel, **c** 6082 perpendicular, **d** 5754 perpendicular
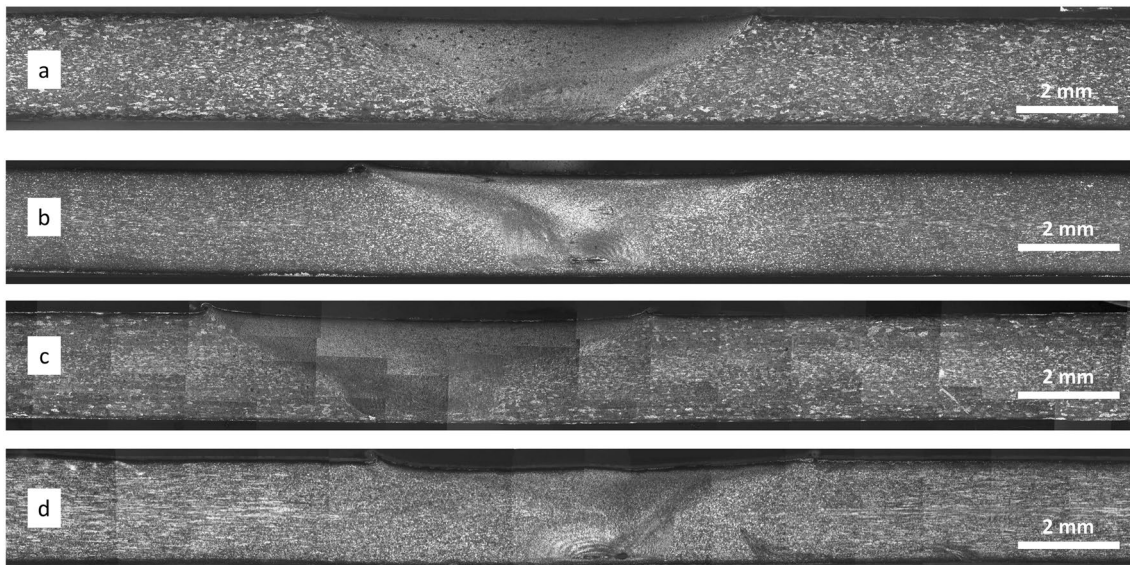
Fig. 6 Macrographies of FSP 6082 and 5754 alloys in cold conditions: **a** 6082 parallel, **b** 5754 parallel, **c** 6082 perpendicular, **d** 5754 perpendicular

where heat and work produced the thermo-mechanically modifications [42, 43].

Different is the case of the 5754 alloy where, at the side of the nugget, a board zone of grain refinement is well visible (see, for example, Fig. 6d). This zone is due to static recrystallization induced by the heat generated during the FSP process, since the 5754 alloy is in the temper state H111, i.e., cold worked. That means that the heat acted upon a structure with high dislocation density and, therefore, easily susceptible to recrystallization.

The results of microhardness measurement are shown in Figs. 7 and 8.

For the 5754 alloy, the hardness does not undergo substantial variation in the welded zone with respect to the base materials, since the grain refinement phenomena compensate for the loss of temper state H111 [44].

The behavior of the 6082 alloy is different: The hardness decreases inside the joint, and the extension of the affected zones is greater in the upper part of the welded zone according to the thermo-mechanical phenomena that occurred during the FSP process. Indeed, it is important to note that Fig. 8 displays significant variations in microhardness compared to Fig. 7. Consequently, more indentations were made, and additional data was collected over the same measurement length to further analyze these differences.

Inside the nugget, the material experiences a complete dynamic recrystallization with grain refinement and dynamic coarsening of precipitates, and these two phenomena have opposite effects on the mechanical properties. The first one leads to the strengthening of the alloy, the second to softening, and in the present case, the effect of precipitates' coarsening prevails, with a worsening of the mechanical properties.
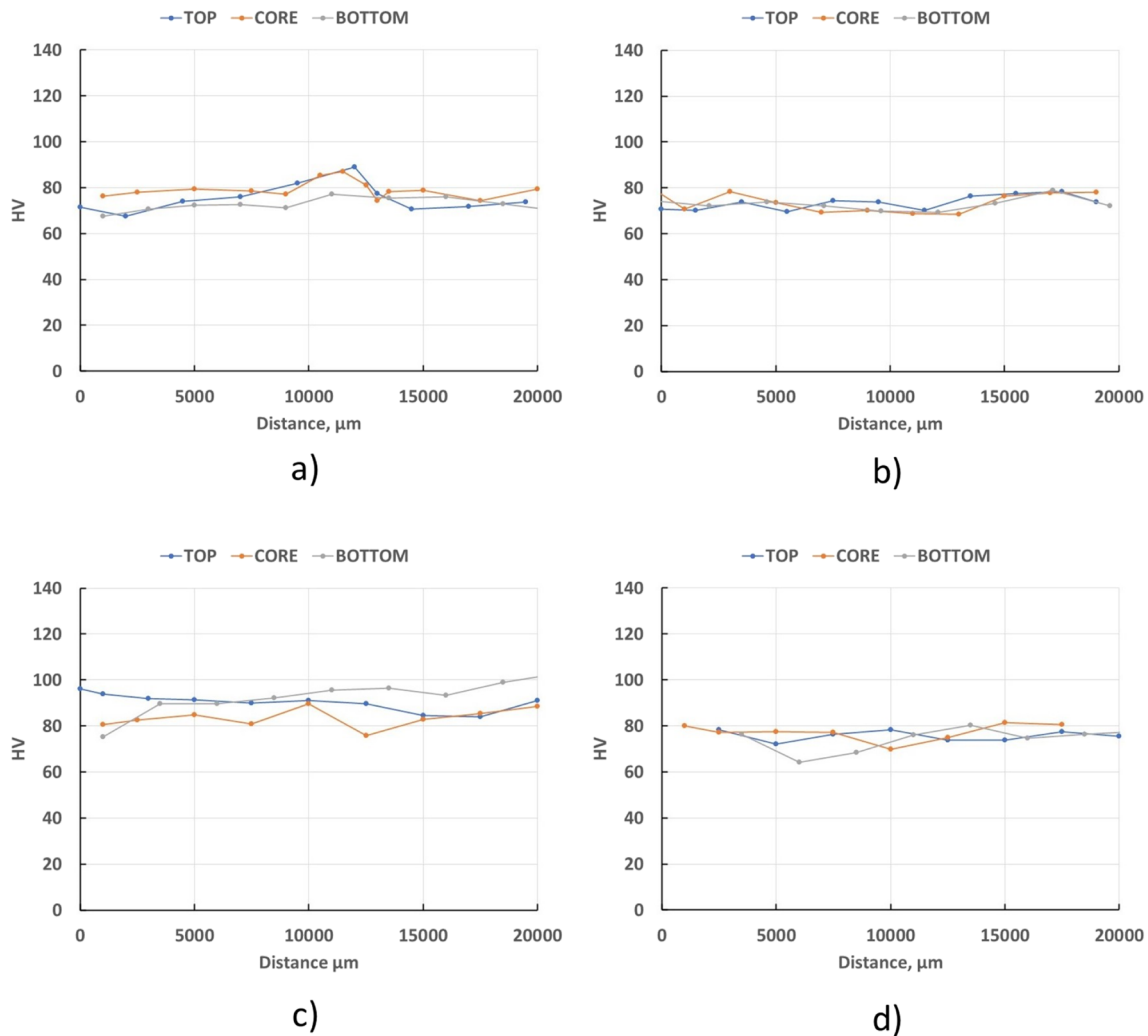
Fig. 7 Microhardness measurements for 5754 alloy in different process conditions: **a** parallel hot, **b** perpendicular hot, **c** parallel cold, **d** perpendicular cold
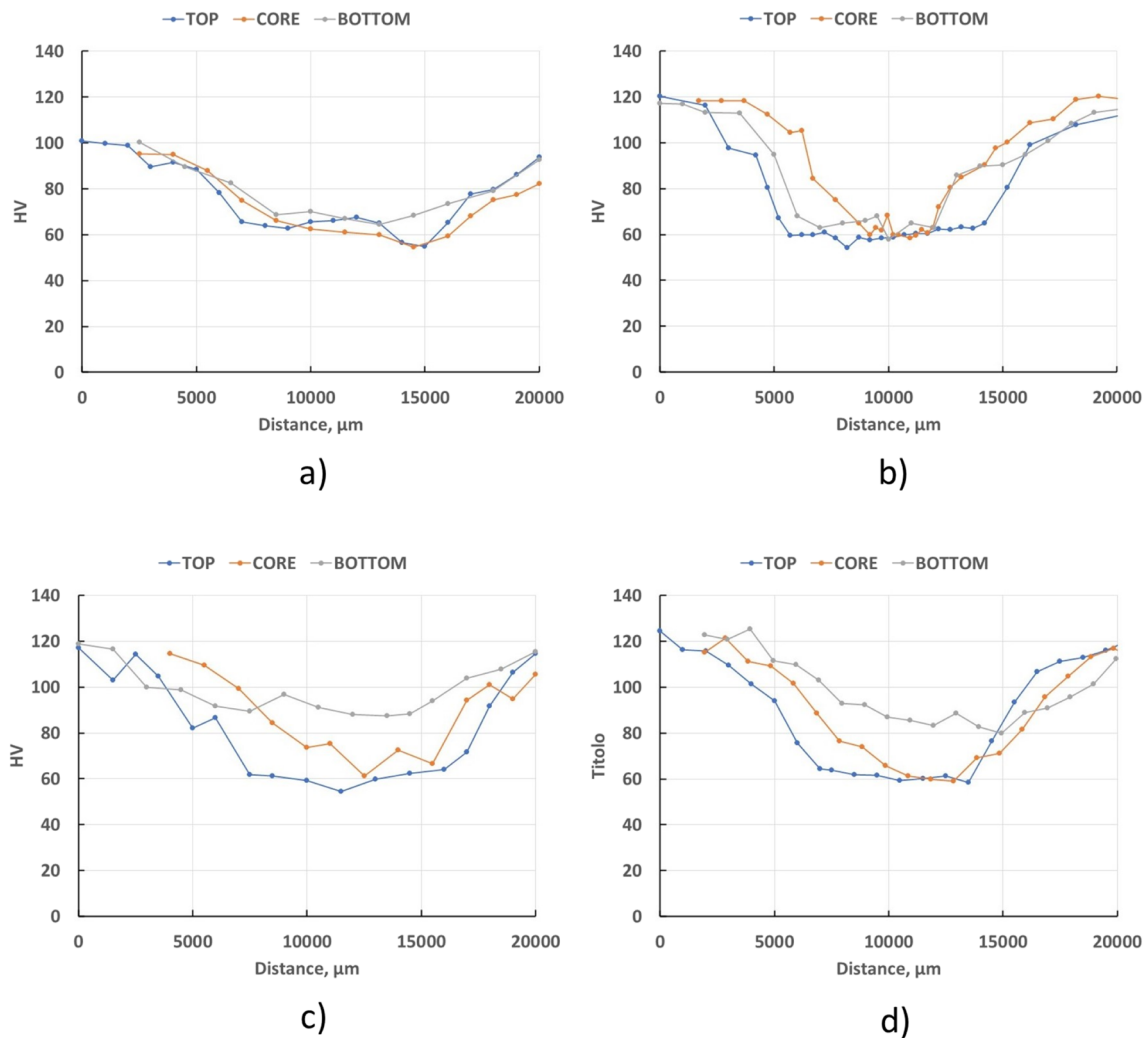
Fig. 8 Microhardness measurements for 6082 alloy in different process conditions: **a** parallel hot, **b** perpendicular hot, **c** parallel cold, **d** perpendicular cold

Also, in the case of the 6082 alloy, the heat generated by the process caused the over-aging of the metal in the areas at the side of the nugget, with a consequent decrease in hardness.

By comparing the micrographs of the two alloys, it can be observed that, in the case of the alloy 5754, the tunnel defect is present in all the process conditions analyzed.

This defect cannot be attributed to an insufficient thermal input, as it is present even in hot conditions, or to an incorrect experimental setup; in fact, the tunnel defect is not present in the case of the alloy 6082.

In agreement with Leitão et al. [17, 45], the plastic behavior of the two alloys is quite different; the 6082 alloy, under process conditions of FSP, is subject to strong over-aging and internal decohesion mechanisms which facilitate the plastic flow. On the contrary, alloy 5754 does not exhibit

a significant softening as well evidenced by the hardness measurements.

The issues in the plastic flow are responsible for the formation of the tunnel defect; moreover, these difficulties are worsened by the fact that the metal sheets used in this experimental work are thin and, therefore, the sections available for the plastic flow are small [46, 47].

Tensile tests were performed on the two alloys treated by the FSP process in all the analyzed conditions, and the results were compared with the base materials. Alloy 5754, as shown in Fig. 9a, has a scattered tensile curve due to the Portevin–Le Chatelier effect; this behavior remains even after the FSP treatment, albeit to a lesser extent.

Again, in the case of the 5754 alloy, the elongation at break and the ultimate strength are comparable with those of the base material in hot conditions.
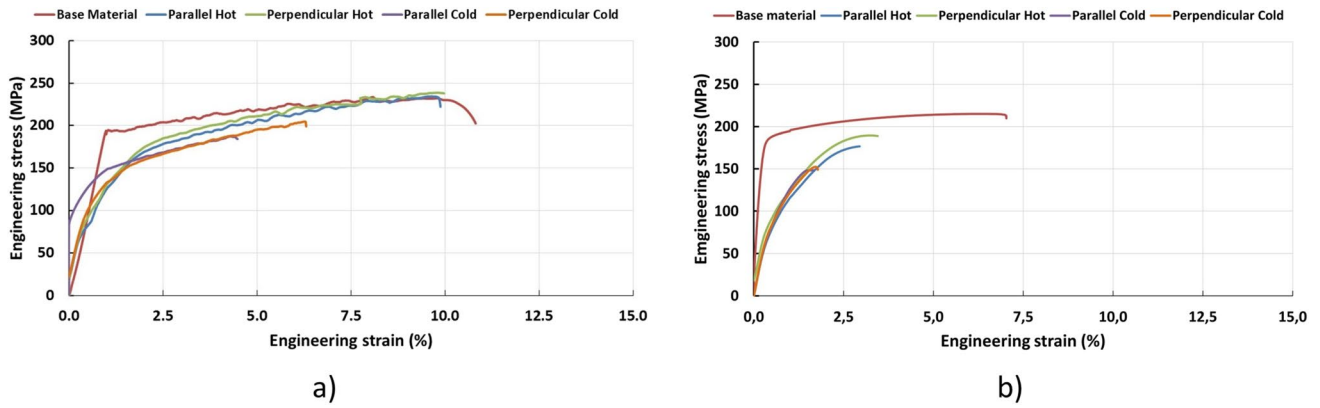
a)

b)

Fig. 9 Tensile test result for base and FSP materials: **a** 5754 alloy, **b** 6082 alloy
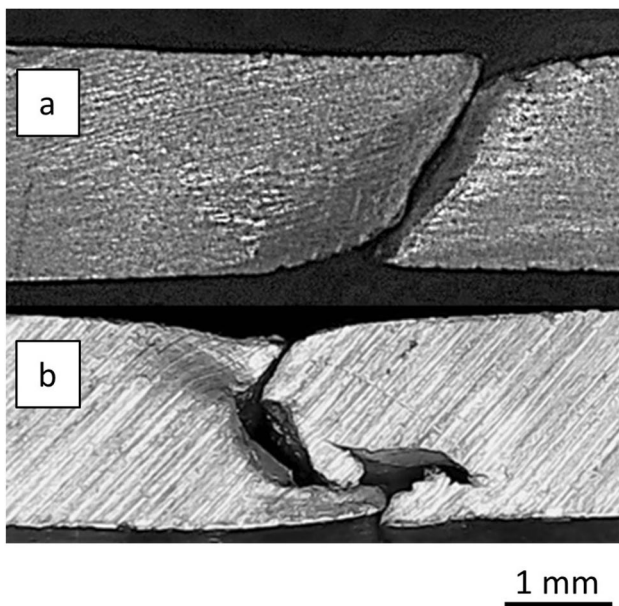

Fig. 10 Different fracture mode observed for 5754 alloy: **a** hot conditions, **b** cold conditions
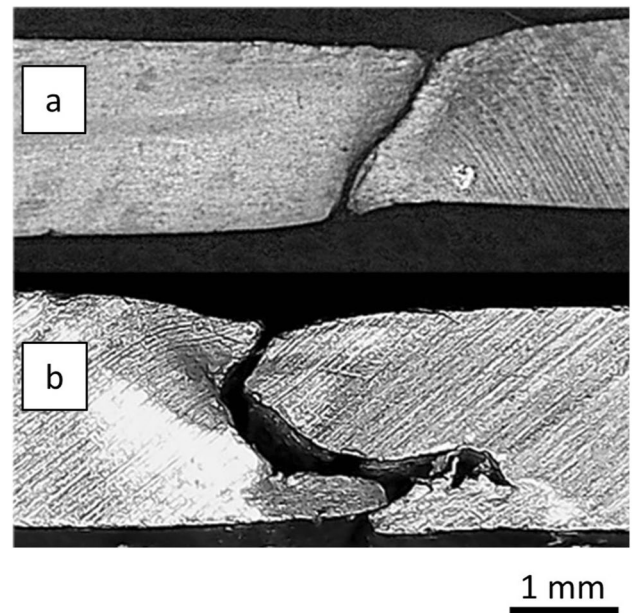

Fig. 11 Different fracture mode observed for 6082 alloy: **a** hot conditions, **b** cold conditions

For the 5754 alloy, the FSP process does not significantly change the mechanical properties; so, during the tensile test, the strain, except for the necking, is uniformly distributed among the entire gage of the specimen. As a consequence, the measured elongation at break is high.

The behavior in cold conditions is different. In this case, the fracture mode changes, as shown in Fig. 10b, where it is clear that the failure occurs inside the nugget by decohesion, and the detrimental effect of the tunnel is evident.

During the FSP process, the material coming from different flows generated by the action of the tool is mixed inside the nugget. If the heat supplied is not enough, these flows do not weld together and represent the weak part of

the joint. On the contrary, in hot conditions, the fracture occurs far from the nugget, as reported in Fig. 10a.

The alloy 6082 shows a different behavior. In this case, the FSP process produced a large area of softening. During the tensile test, the deformation occurs mainly in this area, while the rest of the specimen remains substantially unchanged. Since the engineering strain refers to the entire gage the specimen, in the curves reported in Fig. 9b, the elongation at break is smaller than the base material.

Also, in the case of the alloy 6082, the hot conditions are characterized by higher values of elongation at break and ultimate strength and, as shown in Fig. 11, in cold conditions, the failure occurs inside the nugget due to non-optimal mixing of plasticized metal, whereas in hot conditions, the fracture is
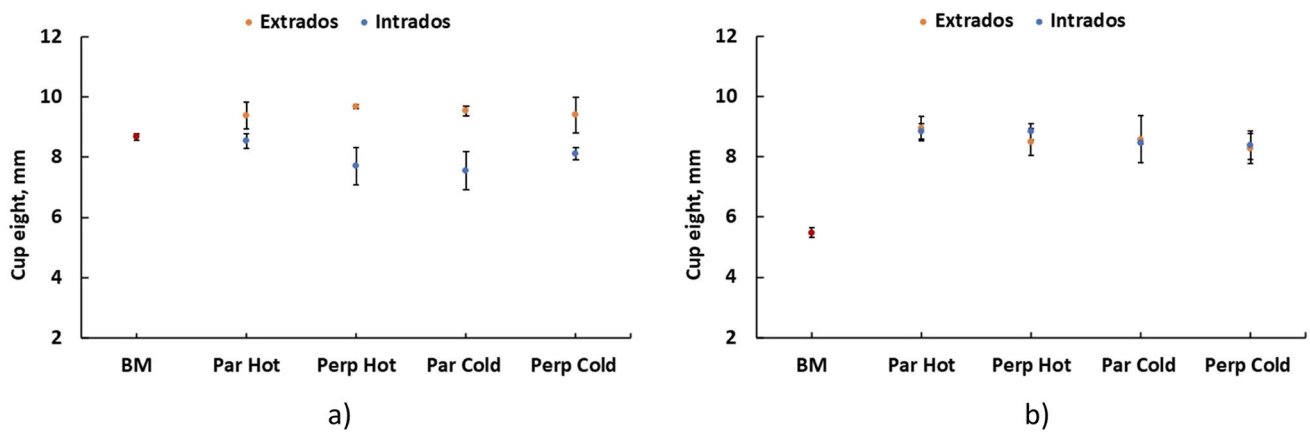
Fig. 12 Results of Erichsen cupping test for **a** 5754 and **b** 6082 alloys

outside the nugget in the HAZ. Although the failure modes may appear similar, the reasons behind them differ. In the case of 5754 alloys, fracture was a result of the tunnel defect. On the other hand, in the case of 6082 alloys, even though this defect was not present, the heat input characteristic of the cold condition was insufficient to ensure optimal material mixing, leading to fracture within the nugget.

The results of the Erichsen cupping test are reported in Fig. 12, where the cup height, i.e., the Erichsen index, at break is plotted versus the different conditions. Some interesting considerations can be made concerning the Erichsen results, also in comparison to the tensile tests. Indeed, it is important to recall that, in the tensile tests, the tested samples varied by changing process parameters, and so considering

Fig. 13 Fracture paths after Erichsen cupping test: **a** 5754 base material, **b** 6082 base material, **c** 5754 hot condition extrados, **d** 5754 cold conditions intrados
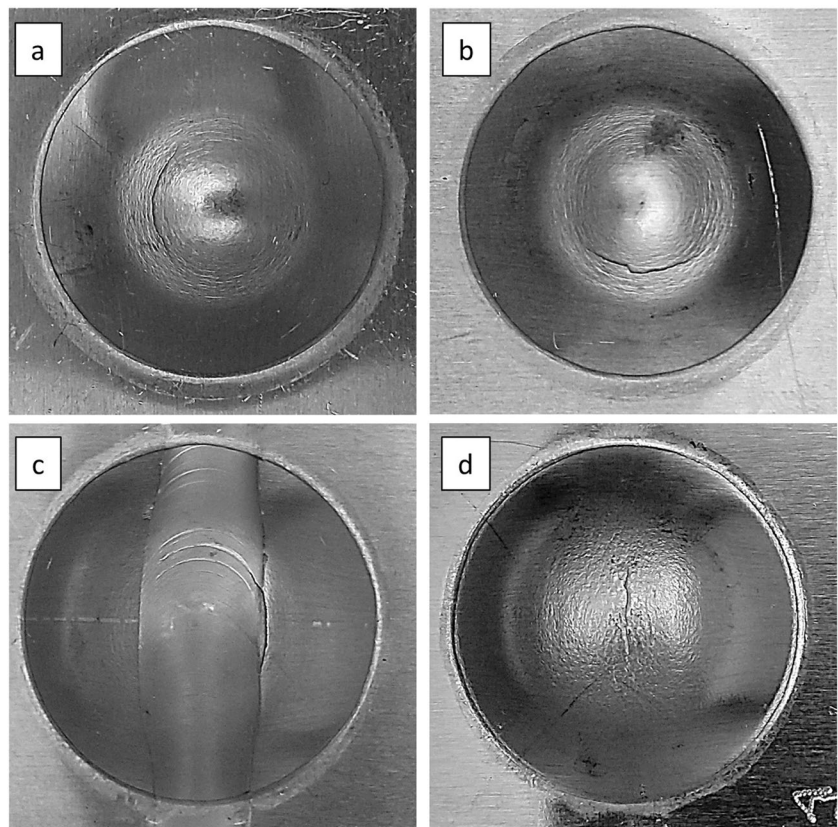
Fig. 14 Fracture paths after Erichsen cupping test: **a** 6082 hot conditions intrados, **b** 6082 hot conditions extrados, **c** 6082 cold conditions extrados, **d** 6082 cold conditions intrados
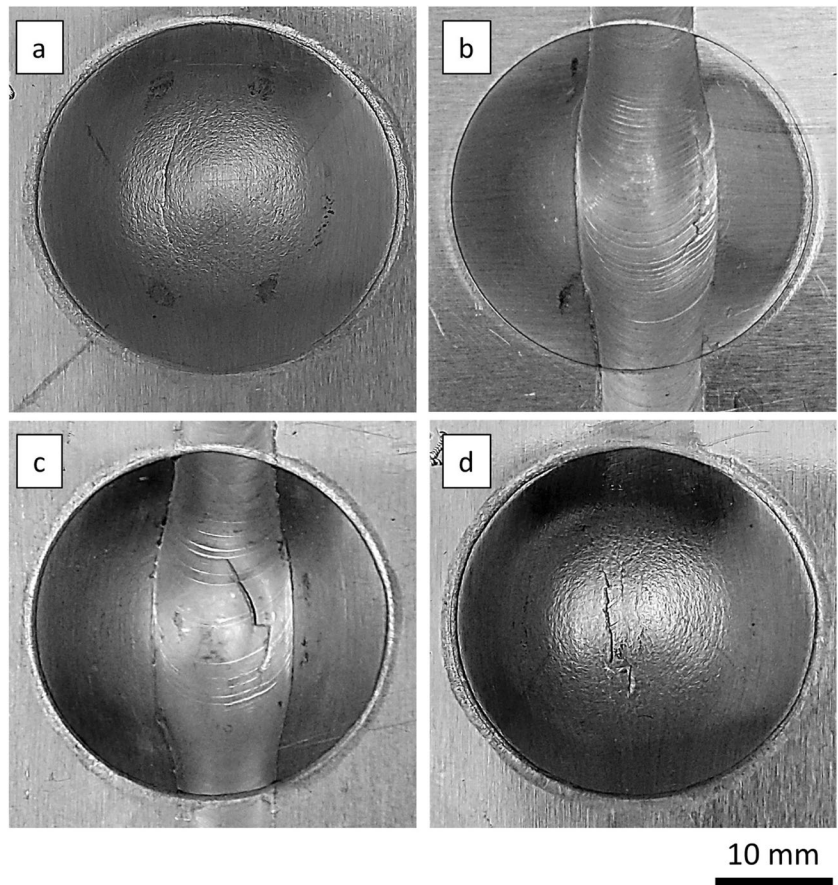

both hot and cold conditions and welding direction, but in the cupping tests, another aspect was considered, i.e., the surface to which the punch was applied. Consequently, each specimen in the aforementioned conditions was tested on both the extrados and intrados of the processed part. This distinction resulted in varying responses in the 5754 alloys.

Looking at Fig. 12, it is possible to note a decrease in cup height concerning all the intrados conditions, and in
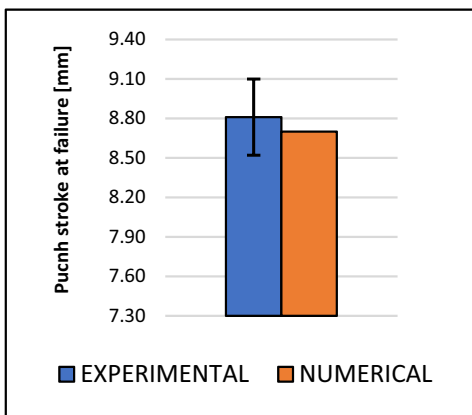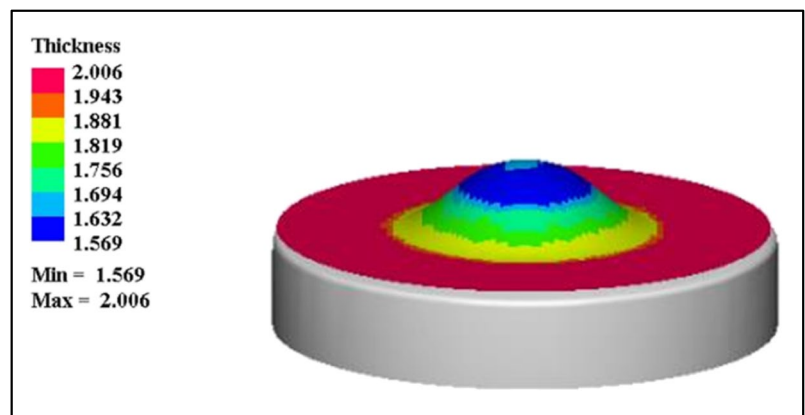
Fig. 15 Numerical results of AA5754-H111 base sheet: **a** comparison between experimental and numerical punch strokes at failure; **b** thickness trend on the sample just before necking (dimensions in mm)
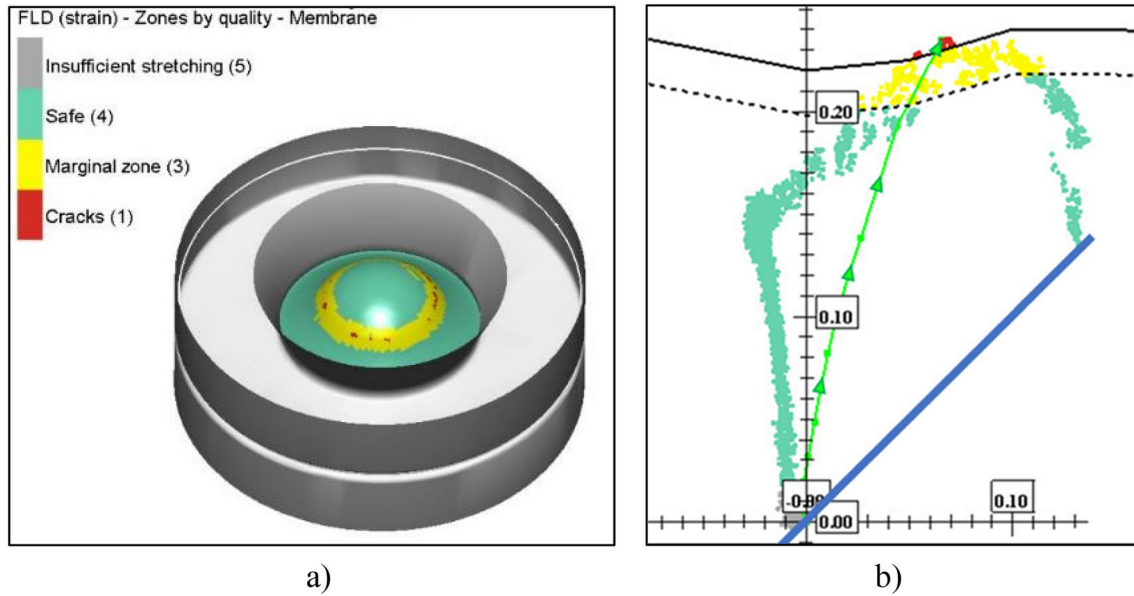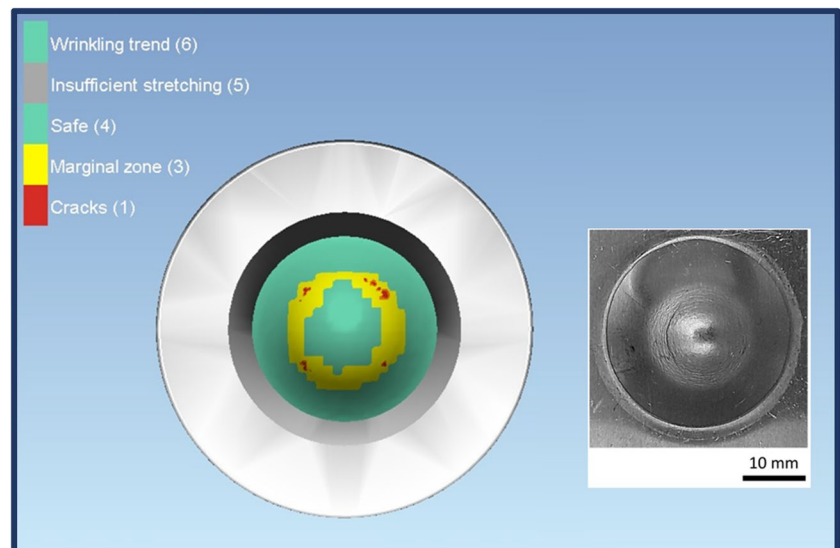
Fig. 16 Forming limit analysis for AA5754-H111 base sheet: **a** location of necking; **b** distribution of local strains on the forming limit diagram and strain path of cracked elements (the blue line represents the $\varepsilon_{max} = \varepsilon_{min}$ condition) [39]

these cases, the fracture occurs in the middle of the weld bead, as reported in Fig. 13d. As previously discussed, the FPS is a challenging process for the 5754 alloy, especially in thin sheets, due to material flowability issues. Tunnel defects were identified in all tested specimens, therefore, the application of high forces involved in the Erichsen tests accentuates the tunnel, creating a notching effect that causes premature failures compared to the base material. However, different findings emerged for extrados conditions. It can be seen that there is no significant change in formability between the untreated condition and the extrados, in agreement with both hardness and tensile test measurements. The same behavior was highlighted by the analysis of the cupping test fractures, illustrated in Fig. 13, in which it is possible to see that in both the 5754 base material and extrados-treated condition, fractures occurred circumferentially around the point of maximum height. In these cases, the reason is related to the fact that the high force exerted during the Erichsen tests led to a reduction and closure of the tunnel defects present in the treated 5754 specimens, making its effect negligible. In other words, beyond cold and hot conditions, intrados- and extrados-treated surfaces strongly

Fig. 17 Experimental–numerical comparison of failure points in extrados for Erichsen cupping test of AA5754 base sheet
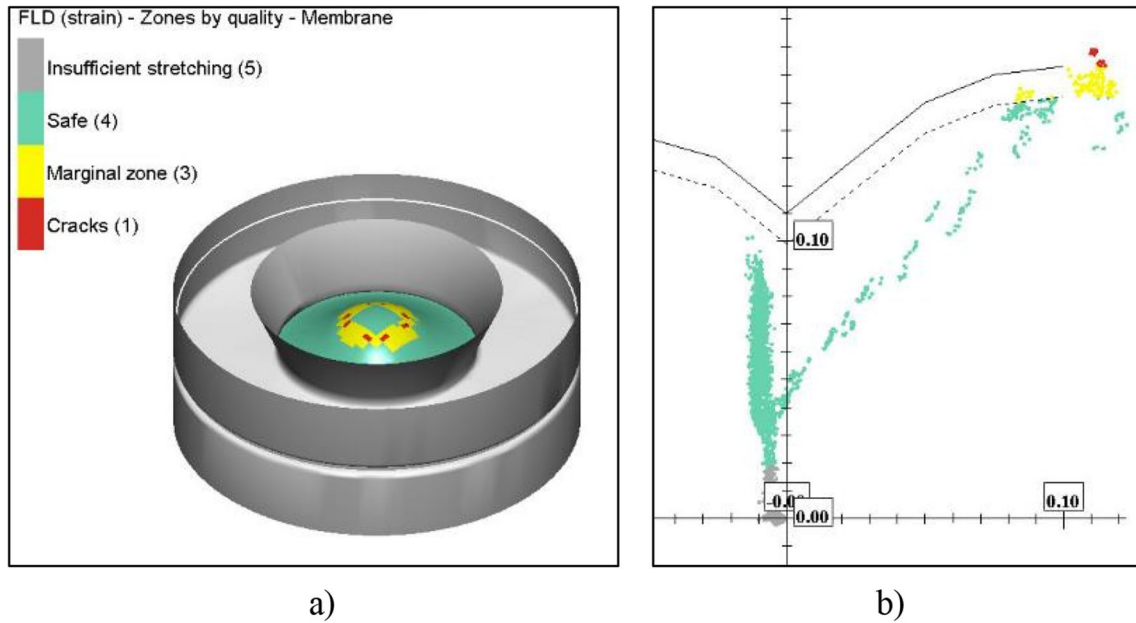
Fig. 18 Forming limit analysis for AA6082-T6 base sheet: **a** location of necking; **b** distribution of local strains on the forming limit diagram [36]

affect the formability of the 5754 alloy, offering potential mitigation for possible defects' effects.

The alloy 6082 is characterized by higher values of cup height with respect to the base materials in all the process conditions analyzed, as reported in Fig. 12. The softening that occurred during the FSP process leads to an increase of ductility and consequently deformability. In hot conditions, the fracture occurs at the side of the weld bead according to the tensile test (see Fig. 14a and b). The weak part of the FSP treated specimens is the heat-affected zone; similarly to

the 5754 alloy in cold conditions, irregular fracture paths are observed as reported in Fig. 14c and d. However, the absence of the defects, such as in the 5754 cases, leads to results comparable in all the processed conditions, both in the extrados and intrados, offering increased formability compared to the base materials, in alignment with the tensile findings.

Furthermore, it can be noticed that the change of the FSP direction to the rolling direction has no influence; indeed, the results obtained for the "parallel" and "perpendicular" conditions are comparable.

Fig. 19 Experimental–numerical comparison of failure points in extrados for Erichsen cupping test of AA6082 base sheet
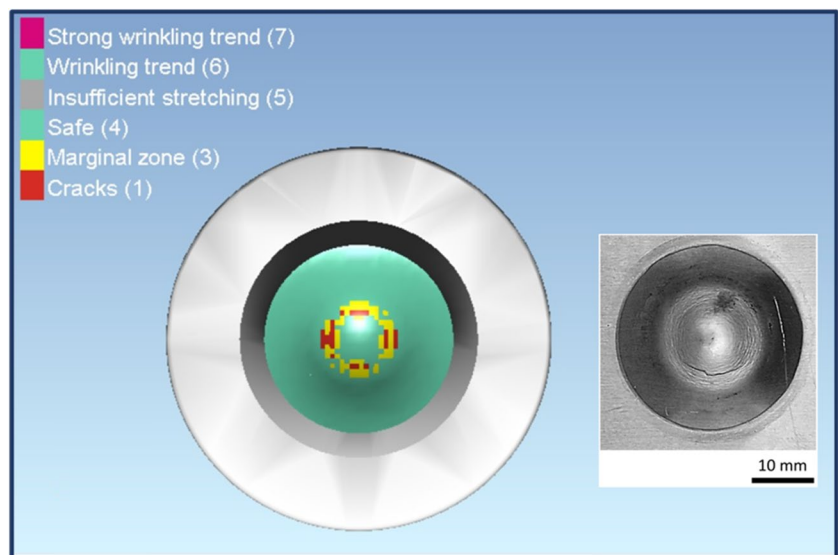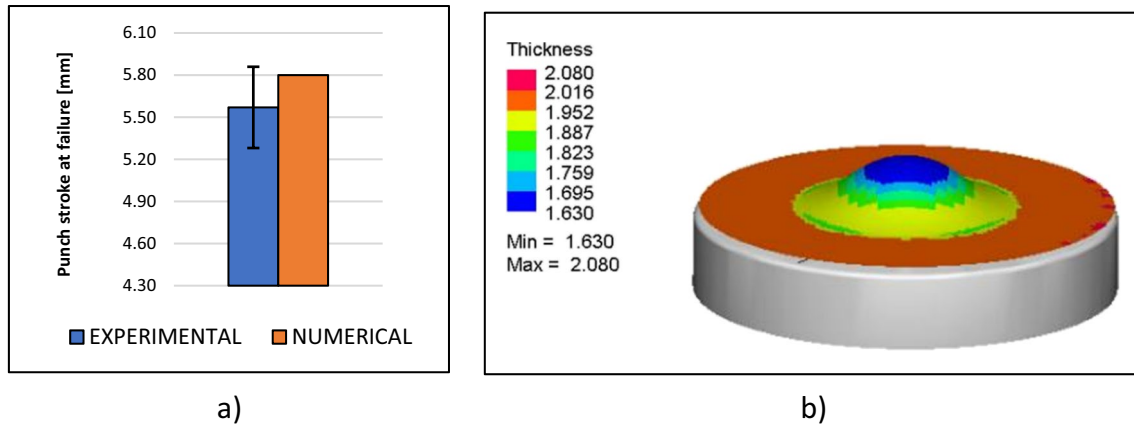
Fig. 20 Numerical results of AA6082-T6 base sheet: **a** comparison between experimental and numerical punch strokes at failure; **b** thickness trend on the sample just before necking (dimensions in mm)

3.2 Numerical results

The adopted approach, being based on shell elements, does not allow for the observation of the variation in failure morphology between extrados and intrados. However, it allowed for the prediction of the maximum height that can be reached by the specimen before failure. Therefore, the obtained results are reported through a comparison between the experimental and numerical punch strokes at failure.

Figure 15a shows the comparison between the experimental and numerical punch strokes at failure for AA5754-H111 base sheet. It is possible to observe that the numerical results were in agreement with the experimental ones. For completeness, Fig. 15b shows the thickness trend on

the sample just before necking. In the case of the absence of friction, the strain path observed on the specimen should be near the $\varepsilon_{max} = \varepsilon_{min}$ line. The presence of friction led to a monoaxial strain state ($\varepsilon_{min} = 0$) near the contour of the contact area between the punch and the sheet, a condition that involves the formation of necking in this critical area. It is possible to observe the location of necking on the specimen in Fig. 16a and the distribution of local strains on the forming limit curve in Fig. 16b. Moreover, a comparison between the experimental and numerical location of failure is shown in Fig. 17.

The results obtained with the AA6082-T6 base sheet were qualitatively similar to those obtained with the AA5754-H111 base sheet. As also experimentally
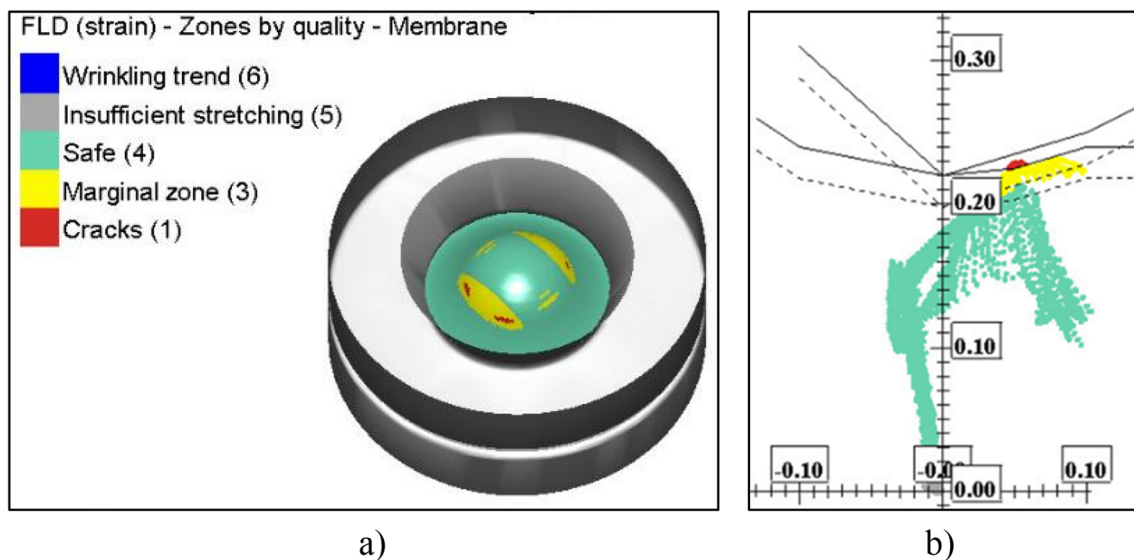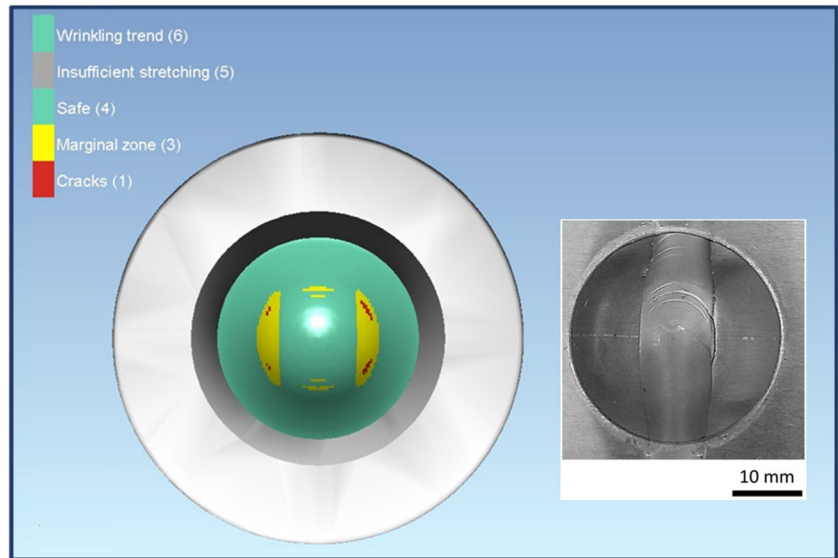

Fig. 21 Forming limit analysis for AA5754-H111 subjected to FSP along rolling direction: **a** location of necking; **b** distribution of local strains on the forming limit diagram [37, 39]

Fig. 22 Experimental–numerical comparison of failure points in extrados for Erichsen cupping test of AA5754 subjected to FSP perpendicularly the rolling direction

observed, this alloy showed lower formability than the previous one. This was evidenced by a lower stroke at failure of punch of about 30%. It is possible to observe the location of the necking on the specimen in Fig. 18a and the distribution of local strains on the forming limit diagram in Fig. 18b. It is possible to state that the smaller contact area between the punch and the specimen, respect the one in AA5754-H111, was due to the different mechanical behavior. This implied a lower influence of friction for the specimens made of AA6082-T6. It is possible to notice this from the fact that the failure points on the forming limit diagram are shifted to the right, towards the biaxial stretching. For completeness, the comparison between experimental and numerical location of failure is reported in Fig. 19.

Figure 20a shows the comparison of the numerical punch strokes at failure with the experimental ones. Although the model tends to slightly overestimate the value of punch stroke at failure, it is possible to state that the numerical results were in agreement with what has been observed experimentally since the obtained numerical value was well-matched with the observed experimental dispersion. For completeness, Fig. 20b shows the thickness trend on the sample just before necking, while Fig. 19 illustrates the comparison between experimental and numerical location of failure. By comparing Fig. 20b with Fig. 15b, it is possible to observe the different formability of the two alloys.

In the case of treated sheets, the specimens could be divided into two cases: specimens treated parallel to the rolling direction and specimens treated perpendicularly to the rolling direction.
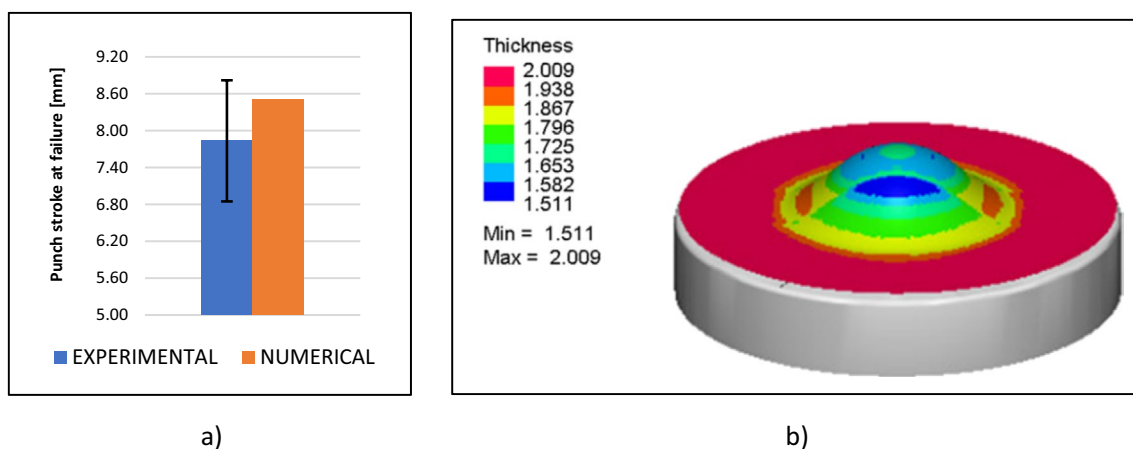

a)

b)

Fig. 23 Numerical results of AA5754-H111 subjected to FSP along rolling direction: **a** comparison between experimental and numerical punch strokes at failure; **b** thickness trend on the sample just before necking (dimensions in mm)
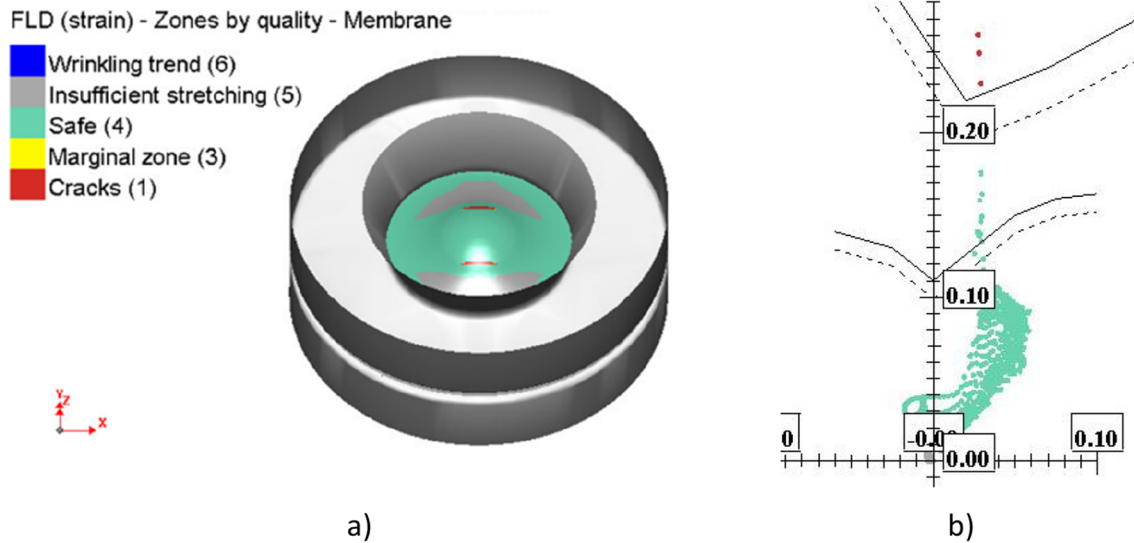
Fig. 24 Forming limit analysis for AA6082-T6 subjected to FSP along rolling direction: **a** location of necking; **b** distribution of local strains on the forming limit diagram [36, 38, 40]

In Fig. 21, it is possible to observe the distribution of local strain for the simulation of AA5754-H111 specimens treated along the rolling direction. The failure numerically occurred at the interface between treated and untreated sheet, near the surface in contact with the punch. A comparison between experimental and numerical location of failure is shown in Fig. 22. However, the proposed approach did not take into account any defects that could be present in the treated area: In this case, the failure would take place inside the treated area, near the contact area with the punch. This is shown by comparing the numerical punch stroke at failure with those experimentally obtained (Fig. 23a). In fact, the obtained numerical value was higher than the average experimental

value, but still compatible with the experimental dispersion observed in the tests. For completeness, Fig. 23b shows the thickness trend on the sample just before necking.

The distribution of local strains for simulation of AA5754-H111 specimens subjected to FSP perpendicularly the rolling direction was similar to that observed for the parallel one. It could be stated that the effect of the rolling direction on AA5754-H111 alloy plates was negligible for forming limit analysis and punch stroke at failure.

In Fig. 24, it is possible to observe the distribution of the local strains for the simulation of AA6082-T6 specimens treated in the parallel direction with respect to the rolling one. The failure occurred at the interface between

Fig. 25 Experimental–numerical comparison of failure points in extrados for Erichsen cupping test of AA6082-T6 subjected to FSP along rolling direction
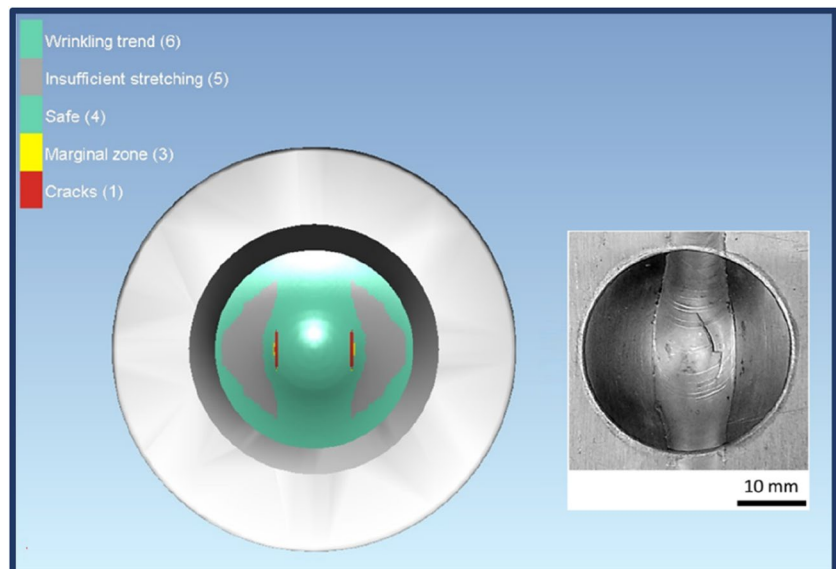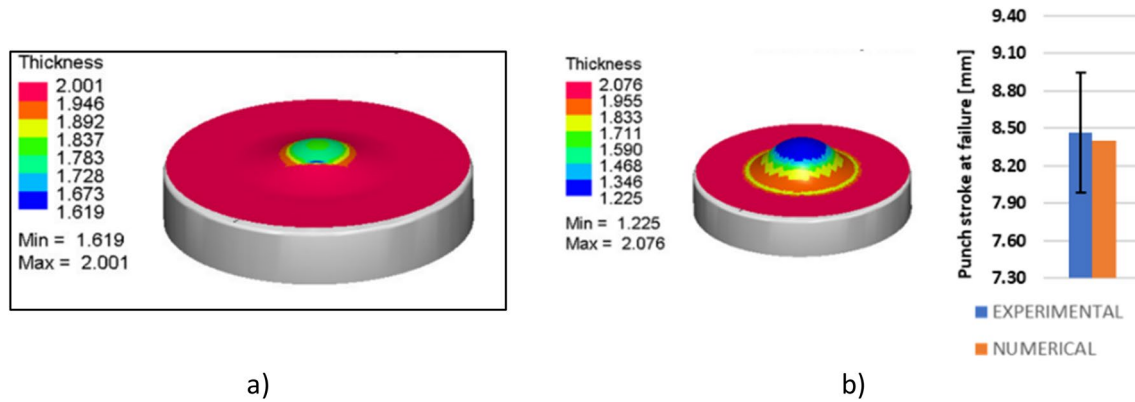
Fig. 26 Thickness trend on the sample just before necking for AA6082-T6 subjected to FSP along rolling direction: **a** modeling the sheet in zone 1 and 3 with a physical state T6; **b** modeling the sheet in zone 1 and zone 3 with a physical state O instead of T6, and comparison between experimental and numerical punch strokes at failure

the treated and untreated area, near the contact area between the punch and the sheet (Fig. 25). In particular, the treated sheet was less deformable than the base sheet, in contrast to what was observed experimentally. This difference may be due to a change in the physical state of the base sheet downstream of the FSP. In this case, the modeling shall consider this mechanical variation. In fact, by modeling the sheet in zone 1 and zone 3 with a physical state O instead of T6, the results obtained are in agreement with what was observed experimentally (Fig. 26b). In conclusion, it can be stated that in the case of AA6082-T6 sheets, the FSP led to an increase in the formability of the sheet but to a decrease in its mechanical strength.

For completeness, Fig. 26a and b show the thickness trend on the sample just before necking, respectively, in case the change in physical state was not considered and was considered.

4 Conclusions

Both alloys 5754 and 6082 present good formability after the FSP process; however, their behavior is quite different.

In the analyzed process conditions, alloy 6082 undergoes internal decohesion and dynamic recrystallization, which facilitate the mixing of material inside the nugget with the absence of defects. The softening is mainly due to the loss of temper state T6 and increases the ductility of the alloy and so the cold formability, as proven by the Erichsen cupping test results.

However, in cold conditions, the analysis of fracture paths indicates the presence inside the nugget of zones where the mixing of materials occurred with difficulty, and these zones are the weak points of the FSP material.

The behavior of the 5754 alloy differs considerably from the 6082 one; in fact, in the first case, the material

flow during FSP is more difficult and, in all the analyzed process conditions, the tunnel defect is present.

The alloy 5754 is not subject to softening; the static and dynamic recrystallizations, occurring during the FSP process due to the combined effect of high temperature and high strain rate, compensate for the loss of temper state H111, and the mechanical behavior and cold formability are comparable to those of base material. Also, in this case, irregular fracture paths are noticed in cold conditions, mainly due to non-optimal mixing inside the nugget and the presence of tunnel defect.

A simplified numerical approach was proposed for the forming limit analysis of treated and untreated sheets, and the numerical results were in good agreement with the experimental ones.

Declarations

Ethics approval and consent to participate The research does not involve human participants and/or animals.

Consent for publication The publication has been approved by all authors.

Competing interests The authors declare no competing interests.

References

1. Ducker Frontier (2020) North American Light Vehicle Aluminum Content and Outlook 2020. 40
2. Frieske B, Kloetzke M, Mauser F (2013) Trends in vehicle concept and key technology development for hybrid and battery electric vehicles. World Electr Veh J 6. https://doi.org/10.3390/wevj6010009
3. Sun X, Li Z, Wang X, Li C (2019) Technology development of electric vehicles: a review. Energies (Basel) 13. https://doi.org/10.3390/en13010090
4. Svendsen A (2020) Aluminum continues unprecedented growth in automotive applications. Light Metal Age 6
5. Napolitano F, El Hassanin A, Scherillo F, Squillace A (2023) FSW of extruded and additively manufactured parts for automotive components. Mater Manuf Process 38. https://doi.org/10.1080/10426914.2023.2176878
6. Hanada E, Takano K, Antoku Y et al (2002) A practical procedure to prevent electromagnetic interference with electronic medical equipment. J Med Syst 26. https://doi.org/10.1023/A:1013094904976
7. Dziubiński M, Drozd A, Adamiec M, Siemionek E (2016) Electromagnetic interference in electrical systems of motor vehicles. In: IOP Conference Series: Materials Science and Engineering
8. Park SK, Hong ST, Park JH et al (2010) Effect of material locations on properties of friction stir welding joints of dissimilar aluminium alloys. Sci Technol Weld Join 15. https://doi.org/10.1179/136217110X12714217309696
9. Dewangan S, Kumar SD, Jha SK, Prakash A (2021) Prediction of formability of MIG and TIG welded joints by Erichsen cupping test and fuzzy-logic technique. Int J Mater Eng Innov 12. https://doi.org/10.1504/IJMATEI.2021.116947
10. Qin G, Ao Z, Chen Y et al (2019) Formability behavior of Al/steel MIG arc brazed-fusion welded joint. J Mater Process Technol 273. https://doi.org/10.1016/j.jmatprotec.2019.116255
11. Zheng K, Politis DJ, Wang L, Lin J (2018) A review on forming techniques for manufacturing lightweight complex—shaped aluminium panel components. Int J Lightweight Mater Manuf 1
12. Yuan SJ, Hu ZL, Wang XS (2012) Formability and microstructural stability of friction stir welded Al alloy tube during subsequent spinning and post weld heat treatment. Mater Sci Eng A 558. https://doi.org/10.1016/j.msea.2012.08.056
13. Hu ZL, Dai ML, Pang Q (2018) Influence of welding combined plastic forming on microstructure stability and mechanical properties of friction stir-welded Al-Cu alloy. J Mater Eng Perform 27. https://doi.org/10.1007/s11665-018-3495-3
14. Pang Q, Zhang JH, Huq MJ, Hu ZL (2019) Characterization of microstructure, mechanical properties and formability for thermomechanical treatment of friction stir welded 2024-O alloys. Mater Sci Eng A 765. https://doi.org/10.1016/j.msea.2019.138303
15. Patel S, Marathe S, Desai K, Raval H (2021) Effect of friction stir welding process parameters on tensile strength and forming height of tailor welded blanks. In: Lecture notes in mechanical engineering
16. Parente M, Safdarian R, Santos AD, et al (2016) A study on the formability of aluminum tailor welded blanks produced by friction stir welding. Int J Adv Manuf Technol 83. https://doi.org/10.1007/s00170-015-7950-0
17. Leitão C, Emílio B, Chaparro BM, Rodrigues DM (2009) Formability of similar and dissimilar friction stir welded AA 5182-H111 and AA 6016-T4 tailored blanks. Mater Des 30. https://doi.org/10.1016/j.matdes.2008.12.005
18. Tayebi P, Fazli A, Asadi P, Soltanpour M (2019) Formability analysis of dissimilar friction stir welded AA 6061 and AA 5083 blanks by SPIF process. CIRP J Manuf Sci Technol 25. https://doi.org/10.1016/j.cirpj.2019.02.002
19. Aktarer SM, Sekban DM, Kucukomeroglu T, Purcek G (2019) Microstructure, mechanical properties and formability of friction stir welded dissimilar materials of IF-steel and 6061 Al alloy. Int J Miner Metall Mater 26. https://doi.org/10.1007/s12613-019-1783-z
20. Pang Q, Wu Z, Hu Z (2022) The influence of process parameters on the preparation of closed-cell aluminum foam by friction stir processing. Int J Adv Manuf Technol 120. https://doi.org/10.1007/s00170-022-08935-5
21. Serio LM, Palumbo D, De Filippis LAC, et al (2016) Effect of friction stir process parameters on the mechanical and thermal behavior of 5754-H111 aluminum plates. Materials 9. https://doi.org/10.3390/ma9030122
22. Zlatanovic DL, Balos S, Bergmann JP, et al (2021) Influence of tool geometry and process parameters on the properties of friction stir spot welded multiple (AA 5754 H111) aluminium sheets. Materials 14. https://doi.org/10.3390/ma14051157
23. Tabanlioğlu E, Hidiroğlu M (2022) Characterization of weldability of 5754-H111 aluminum alloy by friction stir welding (FSW) method
24. Yürük A, Çevik B, Kahraman N (2019) Microstructure and mechanical properties of friction stir welded dissimilar 5754-H111–6013-T6 aluminum alloy joints. Mater./Mater. Test 61. https://doi.org/10.3139/120.111404
25. Rodríguez-Millán M, Vaz-Romero A, Rusinek A, et al (2014) Experimental study on the perforation process of 5754-H111 and 6082-T6 aluminium plates subjected to normal impact by conical, hemispherical and blunt projectiles. Exp Mech 54. https://doi.org/10.1007/s11340-013-9829-z
26. Kah P, Rajan R, Martikainen J, Suoranta R (2015) Investigation of weld defects in friction-stir welding and fusion welding of aluminium alloys. Int J Mech Mater Eng 10
27. Kim YG, Fujii H, Tsumura T, et al (2006) Three defect types in friction stir welding of aluminum die casting alloy. Mater Sci Eng A 415. https://doi.org/10.1016/j.msea.2005.09.072
28. Yi D, Onuma T, Mironov S, et al (2017) Evaluation of heat input during friction stir welding of aluminium alloys. Sci Tech Weld Join 22. https://doi.org/10.1080/13621718.2016.1183079
29. Voort GF Vander (2004) Metals handbook: metallography and microstructures
30. Astarita A, Tucci F, Silvestri AT, et al (2021) Dissimilar friction stir lap welding of AA2198 and AA7075 sheets: forces, microstructure and mechanical properties. Intl J Adv Manuf Technol. https://doi.org/10.1007/s00170-021-07816-7
31. Tucci F, Carlone P, Silvestri AT, et al (2021) Dissimilar friction stir lap welding of AA2198-AA6082: Process analysis and joint characterization. CIRP J Manuf Sci Technol. https://doi.org/10.1016/j.cirpj.2021.09.007

32. ASTM E8 (2010) ASTM E8/E8M standard test methods for tension testing of metallic materials 1. Annual Book of ASTM Standards 4. https://doi.org/10.1520/E0008

33. International Organization for Standardization ISO 20482:2013—Metallic materials—sheet and strip—Erichsen Cupping test

34. Hill R (1948) A theory of the yielding and plastic flow of anisotropic metals. Proc R Soc Lond A Math Phys Sci 193. https://doi.org/10.1098/rspa.1948.0045

35. Marth S, Djebien S, Kajberg J, H ggblad HÅ (2021) Stepwise modelling method for post necking characterisation of anisotropic sheet metal. Model Simul Mat Sci Eng 29. https://doi.org/10.1088/1361-651X/ac2797

36. Çavuşoğlu O, Sürücü Hİ, Toros S, Alkan M (2020) Thickness dependent yielding behavior and formability of AA6082-T6 alloy: experimental observation and modeling. Intl J Adv Manuf Technol 106. https://doi.org/10.1007/s00170-019-04878-6

37. Sojodi S, Basti A, Falahatgar SR, Nasiri SMM (2021) Investigation on the forming limit diagram of AA5754-O alloy by considering strain hardening model, strain path, and through-thickness normal stress. Intl J Adv Manuf Technol 113. https://doi.org/10.1007/s00170-021-06801-4

38. Mrówka-Nowotnik G (2010) Influence of chemical composition variation and heat treatment on microstructure and mechanical properties of 6xxx alloys. Arch Mater Sci Eng 46

39. Mohamed M, Amer M, Shazly M, Masters I (2021) Assessment of different ductile damage models of AA5754 for cold forming. Intl J Adv Manuf Technol 114. https://doi.org/10.1007/s00170-021-06836-7

40. Nghishiyeleke ET, Mashingaidze MM, Ogunmokun AA (2018) Formability characterization of aluminium AA6082-O sheet metal by uniaxial tension and Erichsen cupping tests. Int J Eng Technol 7

41. Sorce FS, Ngo S, Lowe C, Taylor AC (2019) Quantification of coating surface strains in Erichsen cupping tests. J Mater Sci 54. https://doi.org/10.1007/s10853-019-03392-0

42. Buffa G, Fratini L, Impero F, et al (2020) Surface and mechanical characterization of stationary shoulder friction stir welded lap joints: experimental and numerical approach. Intl J Mater Form 13. https://doi.org/10.1007/s12289-020-01574-9

43. Impero F, Scherillo F, Silvestri AT et al (2019) Stationary shoulder friction stir processing: influence of tool wear on surface properties. Key Eng Mater. https://doi.org/10.4028/www.scientific.net/KEM.813.393

44. Sheikh-Ahmad JY, Ozturk F, Jarrar F, Evis Z (2016) Thermal history and microstructure during friction stir welding of Al–Mg alloy. Intl J Adv Manuf Technol 86. https://doi.org/10.1007/s00170-015-8239-z

45. Leitão C, Leal RM, Rodrigues DM et al (2008) Material flow in friction stir welding. Microsc Microanal 14:87–90. https://doi.org/10.1017/S1431927608089472

46. Khan NZ, Siddiquee AN, Khan ZA, Shihab SK (2015) Investigations on tunneling and kissing bond defects in FSW joints for dissimilar aluminum alloys. J Alloys Compd 648. https://doi.org/10.1016/j.jallcom.2015.06.246

47. Tongne A, Desrayaud C, Jahazi M, Feulvarch E (2017) On material flow in friction stir welded Al alloys. J Mater Process Technol 239. https://doi.org/10.1016/j.jmatprotec.2016.08.030